Optical investigation of defects in semi-insulating Tl_6I_4S single crystals

J. A. Peters,[1] M. Sebastian,[1,2] S. Nguyen,[2] Zhifu Liu,[1] Jino Im,[3] A. J. Freeman,[3] M. G. Kanatzidis,[2] and B. W. Wessels[1,*]

[1]*Materials Research Center, Northwestern University, Evanston, Illinois 60208, USA*

[2]*Department of Chemistry, Northwestern University, Evanston, Illinois 60208, USA*

[3]*Department of Physics, Northwestern University, Evanston, Illinois 60208, USA*

(Received 6 September 2013; revised manuscript received 29 April 2014; published 18 July 2014)

Native defect levels in ternary compound Tl_6I_4S single crystals were studied by low-temperature photoluminescence (PL) and photoconductivity (PC) measurements. From the PL measurements, a broad emission band centered at 1.64 eV was observed at low temperatures. The peak can be decomposed using two standard Gaussian functions to reveal two emission bands at 1.55 and 1.66 eV. The PL peak at 1.55 eV is attributed to donor-acceptor pair recombination between a sulphur vacancy (V_S) deep donor ($E_d = 0.57$ eV) and an antisite defect (S_I) shallow acceptor ($E_a = 20$ meV). The 1.66-eV emission band is attributed to self-activated luminescence involving a defect complex and is described using a configuration coordinate model. Within this framework, the 1.66-eV emission band is associated with a S vacancy donor bound to a Tl vacancy acceptor that forms a V_S-V_{Tl} Schottky pair. The photoconductivity spectra show the presence of a deep donor level located at 0.46 eV below the conduction-band edge, in good agreement with that measured by PL spectroscopy.

DOI: 10.1103/PhysRevB.90.035205 PACS number(s): 61.72.−y, 29.40.−n, 72.40.+w, 78.55.Fv

I. INTRODUCTION

The need for hard radiation detectors with good spectroscopic performance that operate at room temperature has led to a widening search for new wide-gap semiconductors. The challenge in designing superior γ-ray detectors is to identify heavy-element (high Z) semiconductors with large band gaps, high electrical resistivity, high mobility-lifetime ($\mu\tau$) products of the charge carriers, and low diffusivity of charged defects to suppress polarization effects [1]. High Z and wide band gap can be found in a number of binary heavy-metal halides, such as TlBr, InI, HgI_2, PbI_2, and BiI_3 [2–6]. Of these, TlBr has emerged as a promising semiconductor radiation detector. The mobility-lifetime ($\mu\tau$) products for both electrons and holes in TlBr are comparable to those in $Cd_{1-x}Zn_xTe$ (CZT), which defines the current state-of-the-art room-temperature semiconductor radiation detector material [7]. However, heavy-metal halides are more ionic than CZT and have much softer lattices. The soft lattice results in low defect formation energies and high concentrations of native defects [8,9]. This leads to a large ionic conductivity [8,10–12] resulting in a severe polarization effect [13]. In addition, carrier transport properties in soft-lattice ionic compounds are generally inferior compared to those strongly bonded covalent semiconductors. It is evident, therefore, that new materials are needed to make advances in gamma ray detection.

Recently, Tl-based ternary semiconductors Tl_6I_4X (X = Se, S) have been demonstrated as promising hard radiation detector materials [14,15]. The concept of lattice hybridization was exploited to design this and other ternary compounds with desired band gaps from binary compounds. By reacting a heavy-metal chalcogenide A_2Q [A = Tl, and Q = Se, S] with a low band gap and a binary halide with a large band gap, one can produce a chalcohalide with high Z exhibiting an intermediate band gap that is highly absorbing for γ rays [14]. Besides having the desired energy gap and mass density, these chalcohalides have also exhibited promising detector properties. For example, Tl_6I_4Se has large $\mu\tau$ products for both electrons (7.1×10^{-3} cm^2/V) and holes (5.9×10^{-4} cm^2/V), and a high resistivity of 4×10^{12} Ω cm along the [001] direction [14]. In addition, the spectral response of Tl_6I_4Se to ^{57}Co γ rays was measured. The detector clearly resolved the 14-, 122-, and 136-keV peaks characteristic of a ^{57}Co γ-ray source, with an energy resolution of 4.7% at FWHM for the 122-keV peak [14].

Ternary chalcohalides offer several other advantages over binary heavy-metal halides. Combining chalcogenides and halides enables more flexibility of tuning properties such as band gap, mobility, and carrier effective mass. However, the flexibility of tuning properties in ternary compounds may come at the expense of complex defect chemistry. Understanding of their defect properties is particularly important for radiation detection. The performance of a semiconductor detector depends on the charge collection efficiency, which is proportional to the $\mu\tau$ product of electrons and holes. Both properties are limited by electrically active defects present in the material. These defects act as trapping or recombination centers that decrease the effective charge collection leading to a degradation of the detector performance.

Experimental and theoretical defect studies can therefore provide important understanding and insights to the performance of various detector materials. First-principles calculations of the defect structure of the ternary chalcohalide Tl_6I_4Se were recently performed [16,17]. The calculations show that native defects are stable where vacancies (V_I, V_{Se}, and V_{Tl}) and antisites (I_{Se} and Se_I) are the dominant defects. The high resistivity of the compound was attributed to compensation between shallow donor antisite defects I_{Se} and shallow metal vacancy acceptors V_{Tl} [16,17]. The excellent $\mu\tau$ product of electrons and holes reported for Tl_6I_4Se was attributed to a combination of small effective masses and effective screening of charged defects. In addition to the theoretical calculations, a recent photoluminescence study on Tl_6I_4Se single crystals found a broad emission band at 1.61 eV due to a donor-acceptor pair recombination involving a

*b-wessels@northwestern.edu

shallow donor level at 52 meV below the conduction-band minimum (CBM) and a deep acceptor level at 290 meV above the valence-band maximum (VBM) [18]. The observed donor-acceptor pair was subsequently attributed to an anti-site pair (I_{Se}-Se_I), whose formation involves an interchange of the positions of a Se ion with its nearest-neighbor I ion [16].

While the electronic structure and defect properties of Tl_6I_4Se have been studied, much less is known about other ternary chalcohalides with potential for radiation detection [19]. We report here on the defect analysis of Tl_6I_4S, a structural analog of Tl_6I_4Se. The Tl_6I_4S compound is semi-insulating and has a room-temperature energy band gap of ~2.03 eV and a resistivity of $\sim 2.6 \times 10^{10}$ Ω cm [15]. The radiation detection response to a Ag x-ray source in the form of a pulse height spectrum was measured. The detector clearly resolved the 22.0- and 22.2-keV peaks, which are characteristic of the K_α lines of Ag. The resolution of the major K_α peak was 2.6% at FWHM [15]. To determine the properties of shallow and deep level defects, photoluminescence (PL) and photoconductivity (PC) measurements were performed on an undoped, single-crystal Tl_6I_4S grown by the Bridgman technique. The study confirms the presence of both shallow and deep level defects in this ternary compound. Donor-acceptor pair recombination between a deep donor and a shallow acceptor accounts for the observed dominant PL spectra of Tl_6I_4S. The photoconductivity spectrum indicates the presence of a deep donor level below the conduction band edge, in good agreement with photoluminescence spectroscopy. The characterization of both shallow and deep levels and the understanding of their effects on electrical properties are of great importance to control and to improve the γ-ray detection properties of Tl_6I_4S.

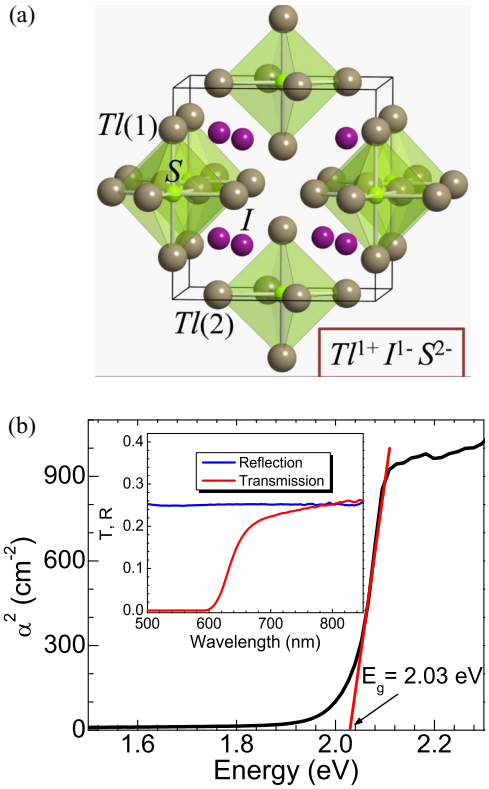

FIG. 1. (Color online) (a) The crystal structure of Tl_6I_4S represented by a ball-and-stick model. Silver, purple, and green balls correspond to Tl, I, and S atoms, respectively. Tl atoms are present in two different lattice sites. (b) Square of absorption coefficient vs. photon energy of a Tl_6I_4S sample. (Inset) Transmission and reflection spectra of Tl_6I_4S.

II. EXPERIMENTAL DETAILS

The compound Tl_6I_4S crystallizes in a tetragonal space group *P4/mnc*, $z = 2$, with unit cell parameters $a = 9.178$ (3) Å and $c = 9.675(1)$ Å [15,20,21]. Figure 1(a) shows the crystal structure of Tl_6I_4S represented by a ball-and-stick model. Silver, purple, and green balls correspond to Tl, I, and S atoms, respectively. Tl atoms are present in two different lattice sites. Synthesis of Tl_6I_4S was performed via reaction of the binary compounds Tl_2S and TlI in the appropriate stoichiometry. Details of crystal synthesis, growth, processing, and characterization are presented elsewhere [15]. Typical dimensions of the crystals suitable for optical measurements are ~4 × 3 × 2 mm [3]. For photoconductivity measurements, samples were prepared by depositing semitransparent gold electrodes (~75-nm thick) on opposite surfaces of the crystal forming a parallel plate configuration.

The band gap of Tl_6I_4S was determined by measuring the transmission and reflection spectra using a UV-VIS spectrometer over the wavelength range of 300–1500 nm with a photomultiplier tube (PMT) (300–860 nm) and InGaAs detector (860–1500 nm). In the transmission configuration, the transmittance T, the reflectance R, and absorption coefficient α are given by

$$T = \frac{(1-R^2)e^{-\alpha d}}{1-R^2e^{-\alpha d}} \quad \text{and}$$

$$\alpha = \frac{1}{d}\ln\left[\frac{(1-R^2)}{2T} + \sqrt{\frac{(1-R)^4}{4T^2} + R^2}\right], \qquad (1)$$

where d is the thickness of the sample. The reflectivity was obtained by normalizing the reflectance of the crystal to that of a silicon reference sample, which has a reflectivity of 0.3 at >1300 nm wavelength. The transmission and reflection spectra versus wavelength are shown in the inset of Fig. 1(b). The band-gap energy was determined by plotting the square of absorption coefficient, α^2, versus photon energy. Extrapolating the linear part of the curve towards lower photon energies and finding the point of interception with the energy axis gives the corresponding direct energy band gap of 2.03 eV at 300 K, shown in Fig. 1(b).

The low-temperature photoluminescence spectra of the Tl_6I_4S crystal were measured from 24–110 K. The samples were cooled using a closed-cycle He cryostat. The excitation source was a He-Cd laser with emission wavelength of 325 nm and a power of 18 mW. The PL spectrum was analyzed with a ¾-m SPEX 1702 monochromator and the signal was detected with a R928 Hamamatsu photomultiplier tube with a phase

sensitive lock-in detection system. For power-dependent PL measurements, a set of calibrated neutral optical density filters was used to limit the intensity of the excitation laser over the range of 0.72 to 18 mW.

The photoconductivity spectra were measured with a lock-in at temperatures ranging from 100 to 300 K using a liquid nitrogen cryostat. Light from a 125 W Xe arc lamp source was focused onto the sample. A Jobin Yvon H20 ¼-m monochromator was used to vary the excitation wavelength from 580–780 nm. Transparency of the thin gold contacts ensured that sufficient incident radiation reached the detector surface. Light absorbed excites electron-hole pairs in direct proportion to the intensity. By applying an electric field of 500 V/cm across the sample, carriers drift towards the anode and cathode, creating an induced charge on the electrodes.

III. RESULTS

A. Excitation intensity and temperature dependence of the photoluminescence spectra

The dependence of the emission processes on excitation intensity and temperature provides information about the nature and mechanism of recombination. Thus the PL spectra from the wide band gap semiconductor Tl_6I_4S were studied at low temperature. Figure 2 shows the PL spectra of Tl_6I_4S at 24 K measured over the energy region of 1.4–2.1 eV and at a constant excitation laser intensity of 18 mW. We observe a wide emission band with a Gaussian line shape with slight asymmetry centered at 1.64 eV and a full width at half maximum (FWHM) of ~0.18 eV. These features are typical of emission bands due to donor-acceptor pair transitions as observed in many ternary semiconductors [22,23]. The broad peak at 1.64 eV can be deconvoluted using two standard Gaussian functions to reveal two emission bands at 1.55 and 1.66 eV, respectively (inset of Fig. 2). We also note that, for the 1.55- and 1.66-eV bands, the emission intensity and peak energy position change with temperature. Furthermore, no near band edge emission was observed.

To better define the recombination processes responsible for the DA luminescent bands of Tl_6I_4S single crystals, the variation of the integrated intensity of the emission bands with excitation laser intensity was measured. Figure 3(a) shows

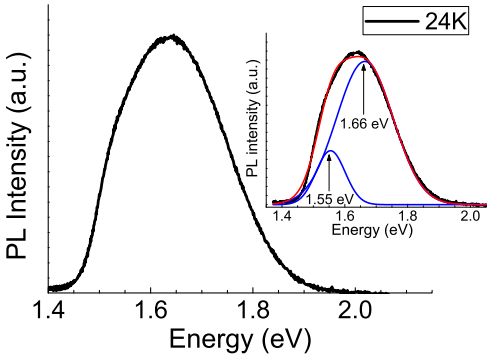

FIG. 2. (Color online) PL spectra of Tl_6I_4S measured at 24 K. (Inset) The deconvoluted broad peak at 1.64 eV showing two emission bands at 1.55 and 1.66 eV, respectively. No near band edge emission is observed.

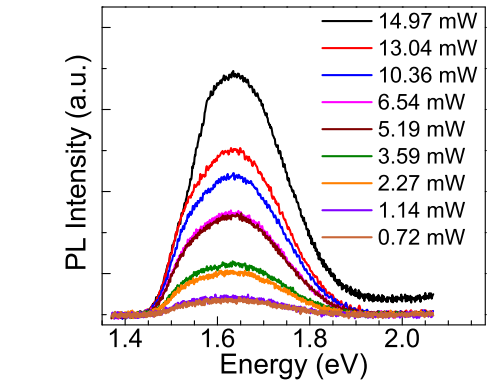

(a)

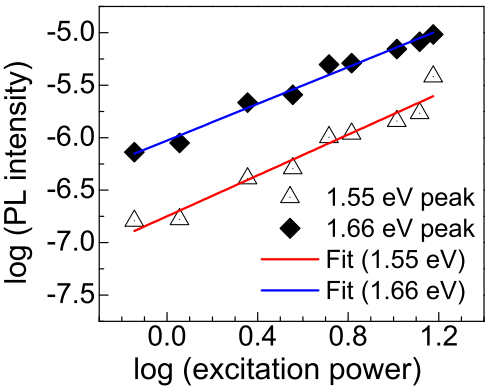

(b)

FIG. 3. (Color online) (a) Excitation intensity dependence of the PL spectra of Tl_6I_4S at 24 K. (b) Excitation intensity dependence of the peak PL intensity of the 1.55- and 1.66-eV bands.

the PL spectra of Tl_6I_4S for nine different laser intensities at 24 K. As in the case of Fig. 2, a decomposition procedure was applied to analyze the behavior of the PL spectra with changing laser excitation intensity. From such an analysis, the peak energy positions and the intensities for the 1.55- and 1.66-eV emission bands with respect to laser excitation are obtained. The energy positions of both peaks blueshift with laser intensity, consistent with inhomogeneously spaced donor-acceptor pairs [22]. Figure 3(b) shows the plots of the logarithmic integrated PL intensities of the 1.55- and 1.66-eV emission bands versus laser excitation intensity. It is well established that the relationship between the integrated PL intensity (I) and excitation power (L) is described by a power law of the form [24]

$$I \propto L^{\gamma}, \tag{2}$$

where γ is a dimensionless exponent. The experimental data is fit to Eq. (2) and the values of γ are 0.87 and 0.97 for the 1.55- and 1.66-eV bands, respectively. For excitation with a photon energy exceeding the band-gap energy, the values of the exponent γ generally fall into one of the following ranges, $0 < \gamma < 1$ or $1 < \gamma < 2$. When $0 < \gamma < 1$, the emission band is attributed to donor-acceptor pair recombination (D, A) or free-to-bound radiative recombination, such as free-hole and neutral-donor recombination (h, D) and free-electron and neutral-acceptor recombination (e, A) [25]. When γ is in the

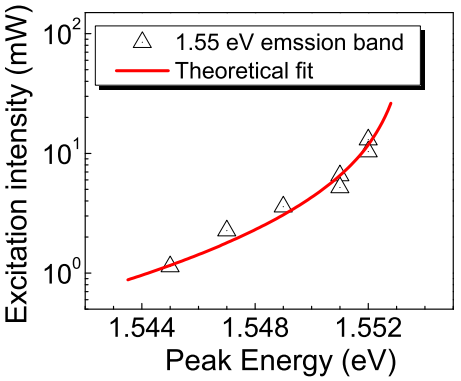

FIG. 4. (Color online) Excitation laser intensity vs peak energy at 24 K. The solid curve gives the theoretical fit using Eq. (5).

range of $1 < \gamma < 2$, the emission band is attributable to bound-exciton transitions [25].

The peak position of the 1.55-eV band changes noticeably with excitation intensity (L) as shown in Fig. 4, thus excluding a free-to-bound transition for which the peak position of the PL band is insensitive to a change in excitation intensity (L) [26]. Thus, the measured values of $\gamma < 1$ support the assignment of the observed emission bands in Tl_6I_4S to donor-acceptor pair recombination. The semilogarithmic plot in Fig. 4 shows the excitation laser intensity as a function of the 1.55-eV emission band peak energy position at 24 K. To obtain the energy values for closely spaced and infinitely distant DAPs, the experimental intensity data in Fig. 4 are then fitted to the following expression [27]:

$$L(E_m) = L_o \frac{(E_m - E_\infty)^3}{(E_B + E_\infty - 2E_m)} \exp\left[-\frac{2(E_B - E_\infty)}{E_m - E_\infty}\right], \quad (3)$$

where L_o is a proportionality constant, E_B the emitted photon energy of a close donor-acceptor pair separated by a shallow impurity Bohr radius (R_B), and E_∞ is the emitted photon energy of an infinitely distant donor-acceptor pair. From a nonlinear least squares fit to the experimental data, E_B and E_∞ are found to be 1.62 ± 0.02 and 1.48 ± 0.01 eV, respectively. Since the emission band peak energy E_m increases from 1.545 to 1.552 eV, E_∞ has lower value than E_m. E_B is the highest DAP emission energy and thus has a higher value than E_m.

To further investigate the recombination mechanism, the PL emission was measured as a function of sample temperature, as shown in Fig. 5(a). Here again, a deconvolution procedure was applied to analyze the behavior of the PL spectra with changing temperature. The integrated intensity of both peaks as a function of reciprocal temperature is shown in Fig. 5(b). A rapid thermal quenching of the PL bands is observed above 30 K. Both the 1.55- and 1.66-eV bands disappear above 100 K. The activation energies of the bands are obtained by fitting the experimental data for the temperature dependence of the integrated intensity of the peaks to the equation [28]:

$$I(T) = \frac{I_0}{1 + \phi_1 T^{3/2} + \phi_2 T^{3/2} \exp(-E_a/k_B T)}, \quad (4)$$

where I_0 is a constant, E_a is the thermal activation energy for thermal quenching, k_B is the Boltzmann constant, φ_1 and

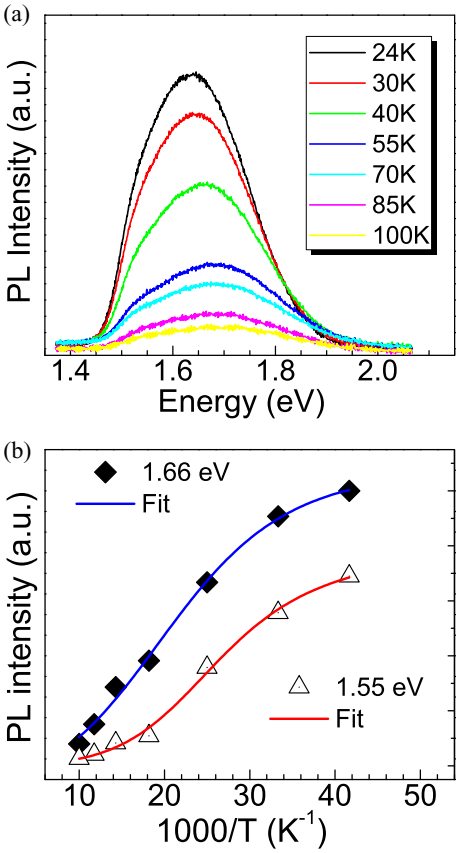

FIG. 5. (Color online) (a) PL spectra of Tl_6I_4S measured in the energy region of 1.4–2.1 eV and in the temperature range of 24–100 K at constant excitation intensity. (b) Integrated intensity of the 1.55- and 1.66-eV peaks as a function of reciprocal temperature.

φ_2 are the fitting parameters associated with the temperature dependence of the capture cross sections of the donor and acceptor impurity levels. The best fit in the temperature range 24–100 K using the above equation gives thermal activation energies of 20 and 11 meV for the peaks at 1.55 and 1.66 eV, respectively.

The temperature dependence of the peak energy for the 1.55- and 1.66-eV emission bands is plotted in Fig. 6(a). The 1.55-eV band shows a very small redshift as the temperature increases. Since the temperature dependence of the band gap of Tl_6I_4S has not been measured, we have assumed that the temperature coefficient of the band-gap energy is negative, as in many ternary semiconductors. Therefore the peak energy due to donor-acceptor pair recombination should also decrease with increasing temperature. The observed small shift of the 1.55-eV band toward lower energies is consistent with the temperature dependence expected for DAP recombination [29,30]. In contrast, however, the temperature dependence of the 1.66-eV emission band shows a different temperature behavior from the 1.55-eV band. The peak energy blueshifts rapidly between 24 and 55 K and continues with a smaller blueshift beyond 55 K up until 100 K, when complete thermal quenching occurs. The magnitude of the peak energy blueshift of the 1.66-eV band is ~36 meV. Such a blueshift in peak energy suggests that the 1.66-eV band is due to emission

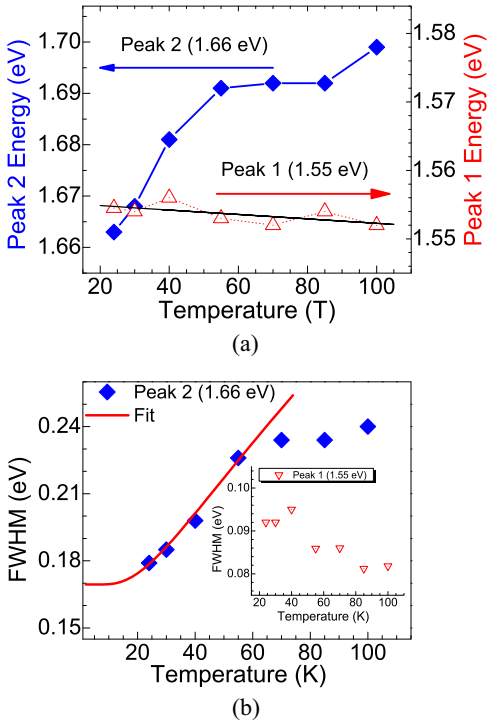

FIG. 6. (Color online) (a) The temperature dependence of the peak energy of the 1.55- and 1.66-eV bands. (b) The temperature dependence of the FWHM line width of the 1.66-eV emission band. The inset shows the FWHM of the 1.55-eV band.

from a donor-acceptor defect complex formed by Coulombic interactions between proximal pairs [31].

According to Klick and Schulman [32], this blue shift of the transition energy with temperature can be described by an electron transition between localized states in a configuration coordinate (CC) diagram, where a ground state is associated with an acceptor level and an excited state is derived from a donor level situated in the band gap of the crystal. When the defect state giving rise to the luminescence is strongly localized, the vibrational energy of the defect contributes considerably to the electron transition energy, and leads to a blueshift with increasing temperature. In addition to the blueshift, the emission undergoes peak broadening with an increase in temperature. The temperature dependence of the FWHM of the 1.55- and 1.66-eV emission bands is shown in Fig. 6(b). We observe that the FWHM of the 1.66-eV emission band increases with increasing temperature, whereas the FWHM of the 1.55-eV band has only a weak dependence on temperature. The temperature dependence of the FWHM, $W(T)$, of the 1.66-eV band can be described by the configuration coordinate model and is given by the equation [31,32]

$$W(T) = W_0 \left[\coth\left(\frac{h\nu_e}{2k_B T} \right) \right]^{1/2}, \qquad (5)$$

where W_0 is the FWHM at 0 K, $h\nu_e$ is the energy of the phonon vibrational mode of the excited state, and k_B is the Boltzmann constant. At $T = 0$, the hyperbolic cotangent equals unity. As shown in Fig. 6(b), the FWHM of the 1.66-eV band shows two distinct behaviors: a low-temperature region from 24–55 K and a high-temperature region above 60 K. Below 60 K the broadening is well described by Eq. (5) whereas above 60 K, the slope of the curve changes and the rate of peak broadening decreases. Previous work on GaS [33] also observed such behavior and the authors indicated that higher excited states can contribute to the high-temperature behavior of the emission bandwidth. Equation (5), however, does not take into account phonon energies associated with multiple excited states. We therefore fit the data to Eq. (5) only in the low-temperature region. The phonon energy of the excited state $h\nu_e$ is 6.1 meV. The constant W_0 of Eq. (5) is 169 meV from the fitting. This value agrees well with the experimental value of 179 meV, the FWHM at low temperature (20 K).

B. Photoconductivity properties

An important characteristic of Tl_6I_4S crystals for radiation detection is its photoconductivity [15]. The photocurrent spectrum for the Tl_6I_4S crystal at 100 K is shown in Fig. 7(a). We observe two main peaks labeled E_1 and E_2 whose maxima are located at 2.07 and 1.61 eV, respectively. Since optical measurements indicate that the band gap of Tl_6I_4S is ~2.03 eV [Fig. 1(b)] at room temperature, the dominant peak at ~2.07 eV (E_1) is attributed to direct transitions from the valence-band maximum to the conduction-band minimum. The second peak labeled E_2 [Fig. 7(a)] is extrinsic in nature and is attributed to photoexcitation of electrons from the valence

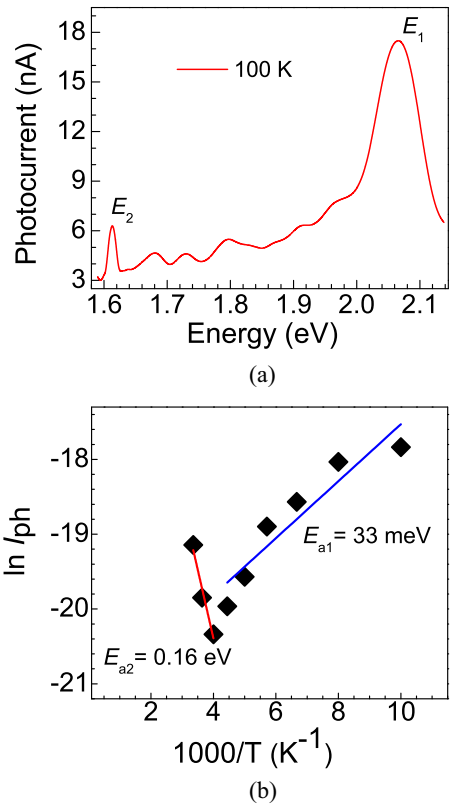

FIG. 7. (Color online) (a) PC spectra of Tl_6I_4S single crystals at 100 K and in the energy range of 1.6–2.15 eV. (b) Variation of ln (I_{ph}) with 1000 T^{-1} for a Tl_6I_4S single crystal.

band into levels associated with defects/impurities within the band gap [34]. Considering that the as-grown crystals have not been intentionally doped, we tentatively attribute the observed peak to native defects.

The temperature dependence of the photocurrent of Tl_6I_4S excited at 1.62 eV is shown in Fig. 7(b). The extrinsic photocurrent displays two different behaviors for different temperature ranges. As can be seen, the photocurrent (I_{ph}) decreases exponentially with increasing temperature from 100 K down to a minimum value at temperature $T_{min} =$ 250 K. Then the photocurrent I_{ph} increases with increasing temperature up to 300 K. In the first temperature region (100 K $\leqslant T <$ 250 K), the photocurrent dependence is given by the equation $I_{ph} = A\exp(E_a/k_BT)$and reveals a photoconductivity activation energy (E_{a1}) of ~33 meV. This is attributed to the thermal quenching of PC between 100 and 250 K. In the second region (250 K $\leqslant T \leqslant$ 300 K), the photocurrent is thermally enhanced, following the equation $I_{ph} = A\exp(-E_a/k_BT)$, with an activation energy of $E_{a2} =$ 0.16 eV.

IV. DISCUSSION

Based on the above analyses of the PL spectra, it is clear that there are two types of emission in the PL spectrum of Tl_6I_4S; one is that of the 1.55-eV band, the other is that of the 1.66-eV band. The peak energy of the 1.55-eV band changes with increasing excitation laser intensity (Fig. 4) and it also shows a small decrease with increasing temperature [Fig. 6(a)]. These results are typical of donor-acceptor pair recombination process, represented by the reaction $D^0 + A^0 \rightarrow \hbar\omega + D^+ + A^-$. The photon emitted in a DAP transition has the energy [23]

$$E(r) = E_g - (E_d + E_a) + \frac{e^2}{4\pi\varepsilon r}, \tag{6}$$

where $E(r)$ is the energy of emitted photon, E_g is the energy band gap, E_d (E_a) is the binding energy of donor (acceptor), respectively, ε is the static dielectric constant, and r is the distance between the donor and the acceptor. The last term in Eq. (6) accounts for the Coulomb interaction between DA pairs and is significant only for very closely spaced pairs. From Eq. (6), two features of the observed data become clear. First, as the temperature is increased, an increase in average pair separation occurs due to thermal emission of charge carriers bound to donor and acceptor levels. Consequently, the peak energies should shift to lower values in addition to the shrinking of the band gap. Second, it is also clear that as the excitation laser intensity is increased, the contribution of closer pairs will increase, leading to the expected blueshift of the peak energy of the emission. Besides the excitation and temperature dependent behavior of DAPs predicted by Eq. (6), the sum of the donor and acceptor binding energies ($E_d + E_a$) can be obtained simply from the determination of the limit $r = \infty$, if E_g is known.

From thermal quenching of the PL spectra, the excitation intensity dependence on PL intensity, and the low-temperature PC spectra, possible processes responsible for the DAP recombination and the photoconductivity impurity peak E_1 can be described. In the proposed scheme, a shallow acceptor level a_1 is located above the top of the valence band. From optical absorption and photoconductivity measurements, the energy band gap at low temperature of Tl_6I_4S is estimated to be ~2.07 eV at 24 K. Consequently, using Eq. (6) and the calculated photon energy value for an infinitely separated DAP E_∞ [calculated from Eq. (3)], the sum of the binding energies of the donor (E_d) and acceptor (E_a) levels can be calculated:

$$(E_d + E_a) = E_g - E_\infty = 2.07\text{ eV} - 1.48\text{ eV} = 0.59\text{ eV}. \tag{7}$$

An activation energy of ~20 meV was deduced from the thermal quenching of the 1.55-eV emission. Since preliminary first-principles calculations indicate that Tl_6I_4S is a p-type semiconductor [35], the measured activation energy is considered to correspond to a shallow acceptor level. Substituting this value of 20 meV into Eq. (7), the binding energy of the donor E_d is calculated to be 0.57 eV indicating that the donor is a deep level. Thus the observed PL emission band at 1.55 eV is attributed to the radiative recombination of an electron occupying a deep donor level d_1 ($E_d = 0.57$ eV) and a hole occupying a shallow acceptor level a_1 ($E_a = 20$ meV). In the case of the PC analysis, an interpretation of the spectral feature at 1.612 eV is that of electron transfer from the valence band to a deep donor level at 0.46 eV below the conduction band, in good agreement with the photoluminescence spectroscopy. Taking into consideration the possible errors in measurement and calculation, the energies at 0.57 eV from the PL and 0.46 eV from the PC are assigned to the same type of defect. Therefore the PL emission peak at 1.55 eV is attributed to DAP recombination between a deep donor and a shallow acceptor. The PL process for the 1.55-eV peak can thus be described as follows: incident photons are absorbed by promoting electrons out of the valence band [indicated by the absorption process in Fig. 8(a)]. The donor defect then captures an electron present in the conduction band. This is followed by a radiative transition of the captured electron back into the acceptor defect [indicated by the recombination process shown in Fig. 8(a)].

In contrast, however, the 1.66-eV emission band shows a different temperature behavior from the 1.55-eV band. As noted earlier, even though the 1.66-eV emission band shows evidence of donor-acceptor recombination, its origin involves a defect complex. This so-called "self-activated" luminescence has been reviewed for defects in ZnS [31] and extended to defects in III-V semiconductor compounds [36,37]. This complex is believed to consist of a nearest-neighbor donor vacancy bound to an acceptor vacancy by a Coulombic force to form a Schottky donor-acceptor pair complex. The ground state of this localized center is derived from a shallow vacancy acceptor, while the excited state originates from a deep vacancy donor. The strong Coulomb attraction between the defect complex leads to a higher ionization energy with respect to the VBM [31,37]. The defect-emission process for the 1.66-eV band can be explained using a configuration coordinate model that takes into account phonon processes [32]. In this model, the potential energy of a luminescent center in an ionic or (partly ionic) semiconductor material is plotted as a function of the configuration coordinate. The term *configuration coordinate* refers to the position of a defect center with that of all the atoms in its immediate vicinity. The ground and excited states of the defect center take the form of parabolic potential wells. In Fig. 8(b), we show a schematic of the CC model for defect

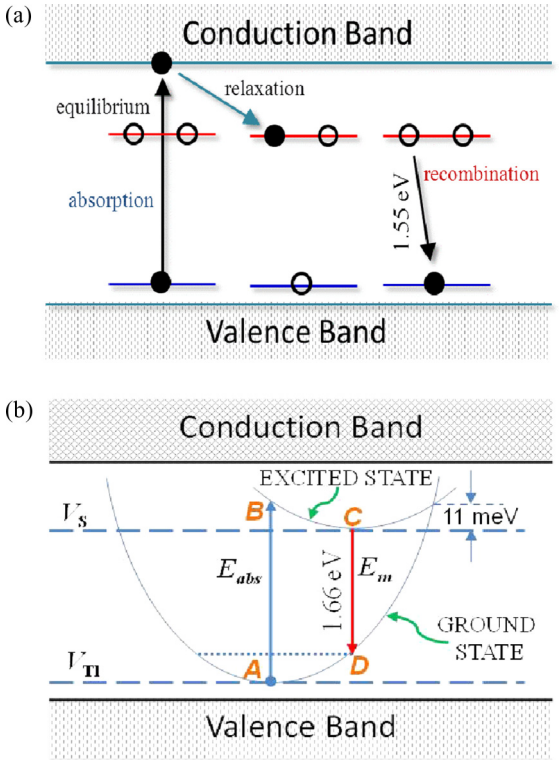

FIG. 8. (Color online) (a) The photoluminescence process responsible for the observed 1.55-eV emission band. (b) The configuration coordinate diagram describing the 1.66-eV luminescence of the defect complex. Also shown are the band gap, and donorlike (V_S) and acceptorlike (V_{Tl}) levels of zero-point energies of the ground and excited states, respectively, which lie within the band gap. E_{ab} and E_{em} are the absorption and emission energies, respectively.

luminescence as applied to our interpretation of the origin of the 1.66-eV luminescence band. In this interpretation, an electron is excited from the equilibrium position of the ground state (point A) to the state at B upon absorbing light. This is indicated by the vertical transition E_{abs} in the CC diagram. Once the electron is in the excited state, the defect center relaxes through lattice vibrations until a new equilibrium is reached at point C. Subsequently, the electron returns to the ground state at point D by emitting light with a photon energy E_m. Finally, the electron relaxes from D to A by again giving up its energy to lattice vibrations. The measured blueshift of the 1.66-eV emission with increasing temperature is attributed to transitions from higher quantized states in the excited level as the occupation of these states increases with temperature. In terms of the CC model, the observed thermal quenching of the 1.66-eV band [Figs. 5(a) and 5(b)] is due to an appreciable population of defects in the excited state which then return to the ground state through nonradiative transitions. Thus the activation energy $E_a = 11$ meV, obtained from the thermal quenching of the PL, is the difference in the energies of the lowest excited state and the intersection point of the excited and the ground state CC curves [Fig. 8(b)]. By correlating the measured temperature and excitation dependence of PL and PC spectra, a more complete picture of the energy-level structure of Tl_6I_4S can be constructed.

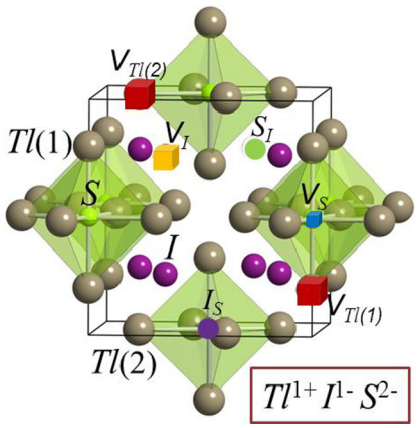

FIG. 9. (Color online) Crystal structure of Tl_6I_4S depicting the types of point defects that can occur in the compound. These include vacancies (V_{Tl}, V_S, and V_I) and antisite disorder (I_S and S_I).

DFT calculations indicate that intrinsic disorder in Tl_6I_4S arises from native defects in the crystal. As shown in Fig. 9, these defects include antisite defects (I_S and S_I) and vacancies (V_{Tl}, V_S, and V_I). Of these point defects, I_S is a shallow donor, S_I and V_{Tl} are shallow acceptors, while V_S is a deep donor [35]. The observed photoconductivity peak at 1.612 eV is attributed to an electron excitation from the valence band to a deep donor level involving a sulphur vacancy (V_S). First-principles calculations show that for the shallow acceptors, the defect formation energy of S_I is lower than that of V_{Tl} by ~0.13 eV. This indicates that the defect concentration of S_I is ~10 times that of V_{Tl}. Based on these calculations, the DAP recombination of the 1.55-eV PL emission is tentatively attributed to the deep vacancy-donor V_S and the shallow antisite-acceptor atom S_I. The DFT calculations [35] further indicate that the localized center V_S-V_{Tl} is a stable complex defect with a high binding energy (0.91 eV) and low formation energy (0.32 eV) due to the strong Coulomb interaction between V_S and V_{Tl}. Thus a "self-activated" luminescence of the localized center V_S-V_{Tl} gives rise to the 1.66-eV PL emission. Using the results from PL, PC, and first-principles DFT calculations, an energy-level diagram of Tl_6I_4S can be constructed as depicted in Fig. 10.

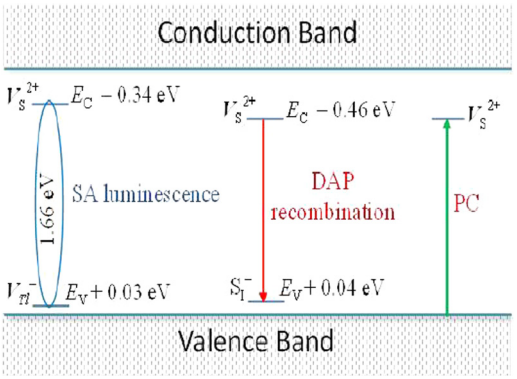

FIG. 10. (Color online) Energy band schematics (not to scale) deduced from the photoluminescence, photoconductivity, and DFT results showing the optical processes at 24 K responsible for the observed peaks at 1.55, 1.61, and 1.66 eV.

V. CONCLUSIONS

Photoluminescence and photoconductivity spectroscopy measurements indicate the presence of both shallow and deep level defects in semi-insulating Tl_6I_4S single crystals. At 24 K, two broad PL bands at 1.55 and 1.66 eV are observed with FWHM of ~100 and 180 meV, respectively. The dependence of the peak energy on excitation intensity and temperature indicate that donor-acceptor pair (DAP) recombination between a deep donor (V_S) and a shallow acceptor (S_I) accounts for the observed emission of the 1.55-eV band. The 1.66-eV emission band is attributed to a "self-activated" luminescence involving a defect complex and is described using a configuration coordinate model. The recombination emission of 1.66 eV is attributed to a Schottky pair defect consisting of a thallium vacancy-acceptor (V_{Tl}) bound to a sulphur vacancy donor (V_S) to form a V_S-V_{Tl} localized center. Photoconductivity spectroscopy indicates the presence of a deep donor level located at 0.46 eV below the conduction-band edge, in good agreement with the photoluminescence spectroscopy. Reduction of these native defects in Tl_6I_4S should lead to semi-insulating semiconductors with higher resistivity and larger mobility-lifetime products, resulting in high efficiency hard radiation detectors.

ACKNOWLEDGMENTS

This work is supported by the Department of Homeland Security with Grant 2010-DN-077-ARI042-02. This work made use of the materials processing and microfabrication facility supported by the MRSEC program of the National Science Foundation (DMR-1121262) at the Materials Research Center of Northwestern University.

[1] A. Kozorezov, V. Gostilo, A. Owens, F. Quarati, M. Shorohov, M. A. Webb, and J. K. Wigmore, J. Appl. Phys. **108**, 064507 (2010).
[2] A. T. Lintereur, W. Qiu, J. C. Nino, and J. E. Baciak, Proc. SPIE **6945**, 694503 (2008).
[3] A. V. Churilov, G. Ciampi, H. Kim, W. M. Higgins, L. J. Cirignano, F. Olschner, V. Biteman, M. Minchello, and K. S. Shah, J. Cryst. Growth **312**, 1221 (2010).
[4] K. S. Shah, J. C. Lund, F. Olschner, L. Moy, and M. R. Squillante, IEEE Trans. Nucl. Sci. **36**, 199 (1989).
[5] K. Hitomi, T. Onodera, and T. Shoji, Nucl. Instrum. Methods Phys. Res. A **579**, 153 (2007).
[6] M. R. Squillante, C. Zhou, J. Zhang, L. P. Moy, and K. S. Shah, IEEE Trans. Nucl. Sci. **40**, 364 (1993).
[7] A. Owens and A. Peacock, Nucl. Instrum. Methods Phys. Res. A **531**, 18 (2004).
[8] M.-H. Du, J. Appl. Phys. **108**, 053506 (2010).
[9] K. Biswas and M.-H. Du, J. Appl. Phys. **109**, 113518 (2011).
[10] G. A. Samara, Phys. Rev. B **23**, 575 (1981).
[11] J. Vaitkus, J. Banys, V. Gostilo, S. Zatoloka, A. Mekys, J. Storasta, and A. Žindulis, Nucl. Instrum. Methods Phys. Res. A **546**, 188 (2005).
[12] C. R. Leao and V. Lordi, Phys. Rev. Lett. **108**, 246604 (2012).
[13] K. Hitomi, Y. Kikuchi, T. Shoji, and K. Ishii, IEEE Trans. Nucl. Sci. **56**, 1859 (2009).
[14] S. Johnsen, Z. Liu, J. A. Peters, J. H. Song, S. Nguyen, C. D. Malliakas, H. Jin, A. J. Freeman, B. W. Wessels, and M. G. Kanatzidis, J. Am. Chem. Soc. **133**, 10030 (2011).
[15] S. L. Nguyen, C. D. Malliakas, L.-D. Zhao, J. A. Peters, Z. Liu, H. Jin, J. Im, M. Sebastian, H. Li, S. Johnsen, J.-H. Song, B. W. Wessels, A. J. Freeman, and M. G. Kanatzidis, Chem. Mater. **25**, 2868 (2013).
[16] K. Biswas, M.-H. Du, and D. J. Singh, Phys. Rev. B **86**, 144108 (2012).
[17] Z. Liu, J. A. Peters, M. Sebastian, M. G. Kanatzidis, J. Im, A. J. Freeman, and B. W. Wessels, Semicond. Sci. Technol. (to be published).
[18] N. K. Cho, J. A. Peters, Z. Liu, B. W. Wessels, S. Johnsen, M. G. Kanatzidis, J. H. Song, H. Jin, and A. Freeman, Semicond. Sci. Technol. **27**, 015016 (2012).
[19] A. C. Wibowo, C. D. Malliakas, Z. Liu, J. A. Peters, M. Sebastian, D.-Y. Chung, B. W. Wessels, and M. G. Kanatzidis, Inorg. Chem. **52**, 7045 (2013); C. D. Malliakas, A. C. Wibowo, Z. Liu, J. A. Peters, M. Sebastian, H. Jin, D.-Y. Chung, A. J. Freeman, B. W. Wessels, and M. G. Kanatzidis, Proc. SPIE **8507**, 85070F (2012).
[20] R. Blachnik and H. A. Dreisbach, Z. Naturforsch. B **36**, 1500 (1981).
[21] R. Blachnik, H. A. Dreisbach, and B. Engelen, Z. Naturforsch. B **38**, 139 (1983).
[22] P. Y. Yu and M. Cordona, *Fundamentals of Semiconductors* (Springer, Berlin, 1995).
[23] P. K. Basu, *Theory of Optical Processes in Semiconductors* (Oxford University Press, New York, 1997).
[24] I. Vurgaftman, J. R. Meyer, and L. R. Ram-Mohan, J. Appl. Phys. **89**, 5815 (2001).
[25] V. A. Fonoberov *et al.*, Phys. Rev. B **73**, 165317 (2006).
[26] S. Levcenko, V. E. Tezlevan, E. Arushanov, S. Schorr, and T. Unold, Phys. Rev. B **86**, 045206 (2012).
[27] N. M. Gasanly, A. Serpenguzel, A. Aydinli, and S. M. A. Baten, J. Lumin. **86**, 39 (2000).
[28] J. Krustok, H. Collan, and K. Hjelt, J. Appl. Phys. **81** 1442 (1997).
[29] S. Shigetomi, T. Ikari, and H. Nakashima, Phys. Status Solidi A **160**, 159 (1997).
[30] A. Aydinli, N. M. Gasanly, I. Yilmaz, and A. Serpenguzel, Semicond. Sci. Technol. **14**, 599 (1999).
[31] S. Shionoya, *Luminescence in Inorganic Compounds*, edited by P. Goldberg (Academic Press, New York, 1966), pp. 205–286; S. Shionoya, T. Koda, K. Era, and H. Fujiwara, J. Phys. Soc. Jpn. **19**, 1157 (1964).
[32] C. C. Klick and J. H. Schulman, *Solid State Physics*, edited by F. Seitz and D. Turnbull, Vol. 5 (Academic, New York, 1957), p. 110.
[33] A. Aydinli, N. M. Gasanly, and K. Gökşen, J. Appl. Phys. **88**, 7144 (2000).
[34] R. Bube, *Photoelectronic Properties of Semiconductors* (Cambridge University Press, Cambridge, 1992).
[35] Jino Im (unpublished).
[36] T. Sauncy, C. P. Palsule, M. Holtz, S. Gangopadhyay, and S. Massie, Phys. Rev. B **53**, 1900 (1996).
[37] E. W. Williams, Phys. Rev. **168**, 922 (1968).